High-mobility two-dimensional electron gas in γ-$Al_2O_3/SrTiO_3$ heterostructures

Xiang-Hong Chen [1], Zhi-Xin Hu [2], Kuang-Hong Gao [1,*] and Zhi-Qing Li [1,†]

[1] *Tianjin Key Laboratory of Low Dimensional Materials Physics and Preparing Technology, Department of Physics, Tianjin University, Tianjin 300354, China*

[2] *Center for Joint Quantum Studies and Department of Physics, Tianjin University, Tianjin 300354, China*

(Received 27 February 2022; revised 9 May 2022; accepted 19 May 2022; published 31 May 2022)

The origin of the two-dimensional electron gas (2DEG) in the interface between γ-Al_2O_3 (GAO) and $SrTiO_3$ (STO) (GAO/STO) as well as the reason for the high mobility of the 2DEG is still in debate. In this paper, the electronic structures of [001]-oriented GAO/STO heterostructures with and without oxygen vacancies are investigated by first-principles calculations based on density functional theory. The calculation results show that the necessary condition for the formation of 2DEG is that the GAO/STO heterostructure have an interface composed of Al and TiO_2 layers. For the heterostructure without oxygen vacancies on the GAO side, the 2DEG originates from the polar discontinuity near the interface, and there is a critical thickness for the GAO film, below which the 2DEG would not present and the heterostructure exhibits insulator characteristics. For the case that only the GAO film contains oxygen vacancies, the polar discontinuity near the interface disappears, but the 2DEG still exists. In this situation, the critical thickness of the GAO film for 2DEG formation does not exist either. When the GAO film and STO substrate both contain oxygen vacancies, it is found that the 2DEG is retained as long as the oxygen vacancies on the STO side are not very close to the interface. The low-temperature mobilities of the 2DEGs in these GAO/STO heterostructures are considered to be governed by the ionized impurity scattering, and ~3 to ~11 times as large as that in $LaAlO_3/SrTiO_3$ heterojunction. The high mobility of the 2DEG is mainly due to the small electron effective mass in GAO/STO heterostructures.

DOI: 10.1103/PhysRevB.105.205437

I. INTRODUCTION

Since the report of the existence of two-dimensional electron gas (2DEG) at the $LaAlO_3/SrTiO_3$ (LAO/STO) interfaces [1], great attention has been paid to the interfaces of STO-based heterostructures [2–16]. The 2DEGs confined in the STO-based heterostructures could reveal a range of unique phenomena including the existence of superconductivity at low temperatures [17,18], electric-field-tuned metal-insulator and superconductor-insulator phase transitions [5,19–21], and the coexistence of ferromagnetism and superconductivity at the interfaces [22,23]. These phenomena make STO-based heterostructures not only have potential applications in novel electronic devices but also be good model systems for fundamental research. Recently, a 2DEG with a low-temperature mobility of $\sim 1.4 \times 10^5$ cm^2/V s, being much higher than that at LAO/STO interfaces, has been realized at the interface between STO and a heteroepitaxial spinel γ-Al_2O_3 (GAO) thin film [11]. This finding shows promise for the applications of the STO-based heterostructures in future electronic devices. Thus it is crucial to understand the formation mechanisms and the origin of the high mobility of the 2DEG at GAO/STO interfaces. However, there has been no consensus on the formation mechanisms of 2DEG in this heterostructure up to now. Some groups believe that the GAO in the heterostructures has polarity, and the charge accumulation is caused by the polar discontinuity at the interface [14–16], while some groups argue that the formation of 2DEG is caused by oxygen vacancies at the interface [24–27]. Besides, the origin of the high mobility remains poorly understood as well [25,28]. To explore why high-mobility 2DEG can be formed at the GAO/STO interfaces, we systematically investigate the electronic structure of GAO/STO heterostructures via first-principles calculations. It is found that the polar discontinuity is the main mechanism for the formation of 2DEG in GAO/STO heterojunctions when there are no oxygen vacancies on the GAO side, while the oxygen vacancies are the main source of the 2DEG for the heterojunction that contains oxygen vacancies on the GAO side. The reasons for the high mobility of the 2DEG in the GAO/STO heterojunctions are also disclosed.

II. CALCULATION METHODS AND HETEROJUNCTION CONSTRUCTION

All calculations are carried out in the framework of density functional theory using first-principles calculation software, the Vienna *ab initio* simulation package. The generalized gradient approximation (GGA) parametrized by Perdew-Burke-Ernzerhof (PBE) plus the on-site Coulomb interaction approach (GGA + U) was used for the exchange-correlation functional. In calculations of the energy band of semiconductors and insulators, the GGA-PBE method generally suffers from the underestimation of the band gap. When the Hubbard

*Corresponding author: khgao@tju.edu.cn
†Corresponding author: zhiqingli@tju.edu.cn

 ©2022 American Physical Society

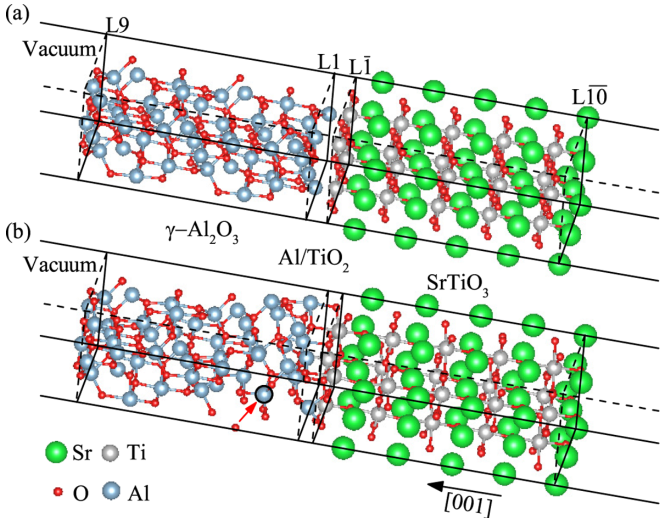

FIG. 1. Schematic structures of $(GAO)_{2.25}/(STO)_5$ heterostructures with Al and TiO_2 layer terminations (a) before and (b) after atomic optimization. The atomic layers on the GAO side are labeled as L1, L2, ..., L9 (the adjacent Al and AlO atomic layers share the same number), and the atomic layers on the STO side are numbered as L$\bar{1}$, L$\bar{2}$, ..., L$\overline{10}$. For clarity, only L1, L9, L$\bar{1}$, and L$\overline{10}$ are shown in the diagram.

interaction parameter U is considered, this defect can be made up to some degree. For the bulk $SrTiO_3$ with perovskite structure, the band gap obtained from the GGA method is 1.83 eV, which is much less than the experimental value (∼3.25 eV [29–31]). When a Hubbard $U = 8.5$ eV is considered for the Ti-3d orbital, the calculated band gap is 2.87 eV while the relaxed lattice constant (3.998 Å) is close to the experimental value (3.93 ± 0.06 Å [28]). Thus, $U = 8.5$ eV is employed in the calculations in this paper. The same U value was used by Lee and Demkov in calculating the electronic structures of LAO/STO heterostructures [32]. A cutoff energy of 500 eV for the plane wave basis set and a Monkhorst-Pack **k**-point mesh of $4 \times 4 \times 1$ were employed. The electronic energy convergence was set to be 10^{-6} eV, and a Gaussian smearing of 0.05 eV was employed for density of states (DOS) calculations.

For GAO/STO heterostructures, considering the experimental result that the 2DEG can only be present at the interface of GAO and the TiO_2-terminated (001) STO substrate [16,33], we construct a 2×2 in-plane STO supercell with the TiO_2 layer terminated on the GAO side and SrO layer terminated on the vacuum side to simulate the [001]-oriented STO substrate. Along the [001] direction, the supercell contains 5 TiO_2 and 5 SrO layers, respectively (see Fig. 1) [34]. Usually, GAO belongs to the defective spinel structure with the space group $Fd\bar{3}m$. In an ideal spinel structure, a unit cell (uc) contains 24 Al atoms and 32 oxygen atoms (8 Al atoms in the tetrahedral sites, 16 Al atoms in the octahedral sites, and 32 O atoms forming a fcc array), and the ratio of cation to anion is 3 : 4. In order to obtain stoichiometric Al_2O_3, 8/3 Al vacancies need to be created per spinel unit cell on average. Therefore, at least 0.75 spinel unit cells are required for the GAO (001) surface to match the Al_2O_3 stoichiometric and vacancy distribution requirements (two Al vacancies). In our calculations, the thickness of GAO slabs varies from 0.75 to 3 uc. For the distribution of Al vacancies in the GAO slab, three aspects are considered [35–39]: (1) Al vacancies preferentially occupy the octahedral positions; (2) the distance between Al vacancies is as great as possible to ensure that the vacancies are distributed as homogeneously as possible in the lattice; and (3) Al vacancies are distributed as deeply as possible inside GAO rather than on its surface. The relaxed lattice constants for bulk GAO are $a = b = c = 7.975$ Å and $\alpha = \beta = \gamma = 90^\circ$. The lattice constant is close to the experimental value (7.911 Å [28,36–38]), which is about twice as much as that of STO (3.998 Å). Thus the lattice mismatch between GAO and STO is ∼0.26%.

Since the structure of GAO can be viewed as an alternating stacking sequence of an Al atomic layer and AlO atomic layer along the [001] direction, both Al/TiO_2 and AlO/TiO_2 interfaces were considered, respectively. Finally, a series of configurations of $(GAO)_n/(STO)_5$ ($n = 0.75$, 1.5, 2.25, and 3) with Al/TiO_2 or AlO/TiO_2 interfaces were constructed (i.e., there are eight configurations) based on the optimized bulk GAO and STO. A vacuum layer with a thickness of 15 Å is inserted between neighbor slabs. Structural optimization was done for all the configurations. All atoms, including the surface layer, are optimized until the residual stress is less than 0.03 eV/Å. It is found that the configurations with the AlO/TiO_2 interface were not significantly changed before and after optimization. However, the case of the configurations with the Al/TiO_2 interface is different. Figures 1(a) and 1(b) show the interface geometry of $(GAO)_{2.25}/(STO)_5$ heterostructure with the Al/TiO_2 interface before and after optimization. For simplicity, we define the $(GAO)_{2.25}/(STO)_5$ heterostructure with the Al/TiO_2 interface as configuration 1. It is found the structure (lattice constants) of the atomic layers far from the interface has little change before and after relaxation, while the structure of the atomic layers near the interface is distorted. Particularly, the positions of atoms in the three Al layers and AlO layers near the interface have been changed. For example, the Al atom (pointed out by arrow) in the L2 AlO layer should be at the center of the octahedron, while it deviates from that position after optimization. As a consequence, the local lattice constants along the [100] and [010] directions in L1 to L3 AlO layers on the GAO side increase by ∼1.1% and ∼1.4%, respectively. On the STO side, the local lattice constant along [100] in the L$\bar{1}$ TiO_2 layer increase by 1.4%, while it decreases by 1.6% along [010]. Although the structure distortion occurs in the GAO slab near the interface, the alternating structure of the octahedral cation and tetrahedral cation along the [001] direction is still retained, which is consistent with the experimental results [24,40].

III. RESULTS AND DISCUSSION

A. GAO/STO heterostructures without oxygen vacancies

First, we calculated the electron DOS of the GAO/STO heterostructures with the eight configurations mentioned above. It is found that the Fermi levels of the heterostructures with the AlO/TiO_2 interface lie in the band gap no matter how thick the GAO layer is. Thus the AlO-layer-terminated heterostructures are always in the insulating state. The situation

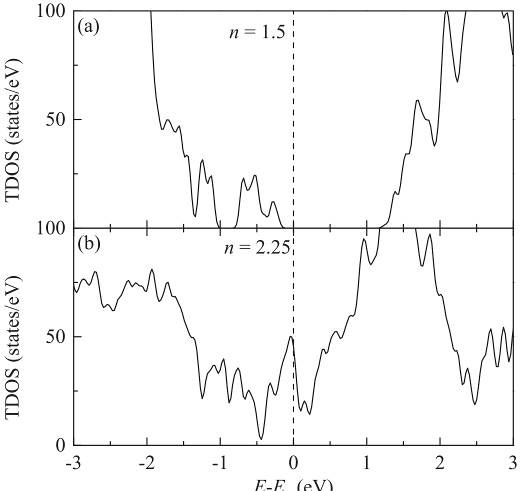

FIG. 2. The DOS of $(GAO)_n/(STO)_5$ heterostructures with Al/TiO_2 interface for (a) $n = 1.5$ and (b) $n = 2.25$.

on GAO/STO heterostructures with the Al/TiO_2 interface is different. Figures 2(a) and 2(b) show the total DOS of the $(GAO)_n/(STO)_5$ heterostructures with the Al/TiO_2 interface for $n = 1.5$ and 2.25, respectively. The Fermi level for the $n = 1.5$ heterostructure lies in the band gap, indicating that the $n = 1.5$ heterostructure is an insulator in the band structure. The band structure of the $n = 0.75$ heterostructure is similar to that of the $n = 1.5$. In contrast, the gap vanishes entirely and apparent nonzero DOS can be observed near the Fermi level for the $n = 2.25$ heterostructure [Fig. 2(b)]. That is, the $n = 2.25$ heterostructure possesses the band structure of metals and a similar phenomenon is also observed in the $n = 3$ heterostructure. Therefore, the 2DEG will be formed in GAO/STO heterostructures with the Al/TiO_2 interface when the thickness of GAO is greater than 1.5 uc ($n > 1.5$), and the critical thickness of GAO for the presence of 2DEG in GAO/STO heterostructures is ∼1.5 uc. Since the results in the $n = 3$ heterostructure are similar to those in the $n = 2.25$, we will systematically present the results and discussions concerning the GAO/STO heterostructures with the Al/TiO_2 interface and $n = 2.25$ below.

Figure 3(a) shows the partial density of states projected onto atomic planes in the STO and GAO of the $n = 2.25$ heterostructure (configuration 1). From this figure, one can see that the states at the top of the valence band are mainly contributed by the AlO layers, and the related valence-band edge gradually shifts upward with increasing layer number

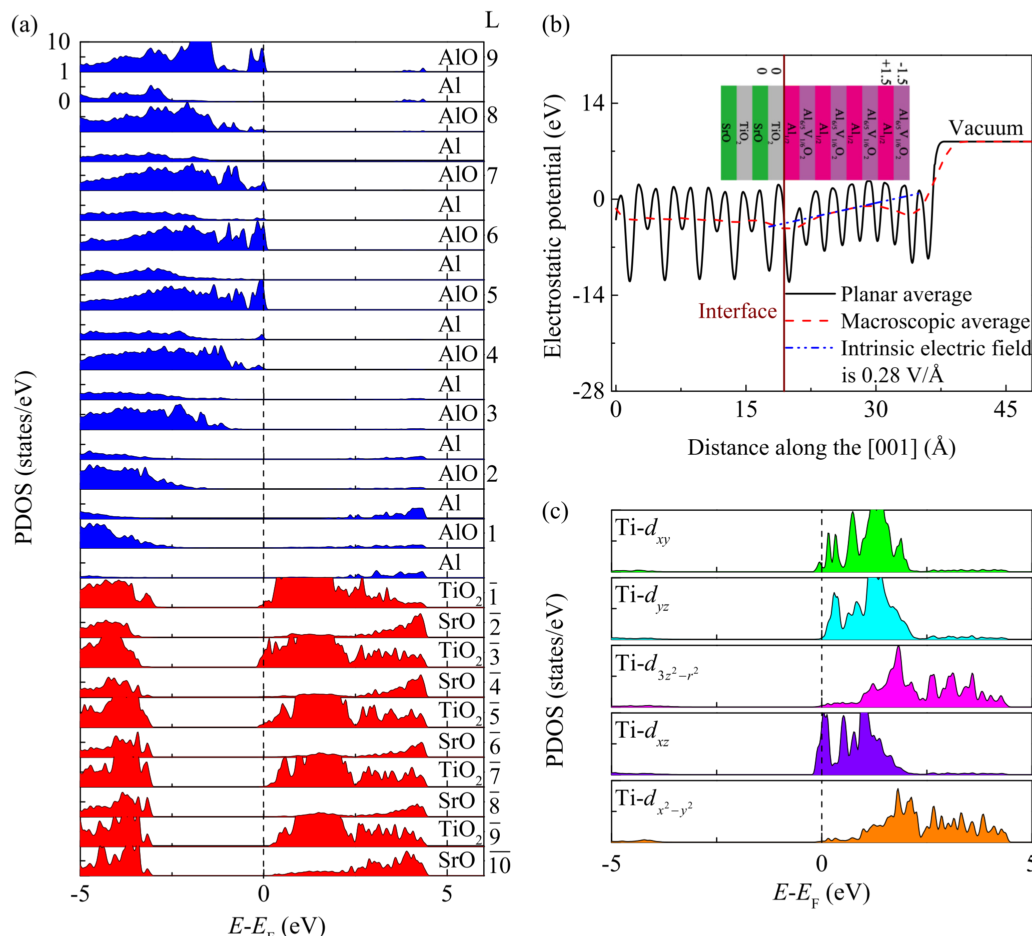

FIG. 3. (a) The partial density of states projected onto atomic planes in the STO and GAO of configuration 1. (b) The plane-average electrostatic potential (solid line) and macroscopic-average electrostatic potential (dashed line) of configuration 1. Inset: A sketch of the GAO/STO heterostructure. (c) The orbitally resolved partial DOS for $L\bar{3}$ TiO_2 layer in STO.

from L1 to L5 layers (i.e., the farther the AlO layer is from the interface, the greater the related valence-band edge moves upward). On the other hand, the conduction-band edge of the L$\bar{1}$ to L$\bar{5}$ TiO_2 layers is lower than the Fermi level, and thus the valence band of the L5 to L9 AlO layers has an overlap with the conduction band of the L$\bar{1}$ to L$\bar{5}$ TiO_2 layers. These band overlaps cause the electrons to be transferred from the former to the latter, resulting in incompletely filled bands. Thus, the 2DEG is formed near the interface. We note in passing that we also calculated the electronic structure of the $(GAO)_{2.25}/(STO)_{7.5}/(GAO)_{2.25}$ symmetric heterostructure, in which the (001) STO slab with thickness $t = 7.5$ uc has two TiO_2 terminations and the GAO slabs are both terminated on Al layers at the interfaces of the heterostructure. It is found that the DOS spectra (not shown) of the heterostructure are almost left-right symmetric and the left half (or the right half) of the DOS spectra is almost identical to that shown in Fig. 3(a).

As for the origin of the band overlap, the polar discontinuity at GAO/STO interfaces is the most likely candidate. We have known that the GAO slab in optimized configuration 1 maintains the alternating structure of the octahedral cation and tetrahedral cation along the [001] direction [Fig. 1(b)]. The homogeneous distribution of aluminum vacancies on the octahedral site leads to each AlO layer having a $-1.5e$ charge, and then each tetrahedral layer containing only aluminum cations has a charge of $+1.5e$. Therefore, the GAO can be interpreted as stacking of atomic layers with an alternating charge of $\sigma = \pm 1.5e$ [41] [see the inset of Fig. 3(b)], and the GAO is a polar crystal with nonvanishing electric dipole moment in the [001] direction [41,42]. Figure 3(b) shows the plane-average (solid curve) and macroscopic-average (dashed curve) electrostatic potential of configuration 1 as a function of the position in the direction normal to the interface. The potential in GAO increases gradually along the z direction due to the alternating polarity of the atomic layers, indicating the presence of a polar electric field in GAO. Consequently, the polar electric field causes an upward shift of the valence-band edge. By a linear fitting of the macroscopic-average electrostatic potential [43], a polar electric field of 0.28 V/Å is obtained. Using the electric field of 0.28 V/Å and the GGA + U band gap of 2.87 eV for STO, one can obtain the critical thickness of GAO that is ∼1.3 uc. This value is close to our result mentioned above. If the electric field of 0.28 V/Å was completely compensated, 0.92 electrons per unit-cell area (e/A) (equivalently, carrier concentration value is 1.47×10^{14} cm^{-2}) should be transferred from GAO to STO. Integrating the DOS spectra from the bottom of the conduction band to the Fermi level, one can obtain the carrier concentration n of the heterojunction. The carrier concentration in the slab with configuration 1 is 1.14×10^{14} cm^{-2}, which is close to the density of the compensating electrons mentioned above. This result confirms that the polar discontinuity induces the formation of 2DEG in configuration 1, which is similar to the case in LAO/STO heterostructures [44,45]. The slight deviation between the two values could be caused by the ionic polarization that partially screens the polar electric field in GAO [46]. And we find that 66.4% of the electrons occupy the Ti-3d orbitals of the L$\bar{3}$ TiO_2 layer. Therefore, the metallic state of configuration 1 is mainly contributed by the L$\bar{3}$ TiO_2 layer.

Figure 3(c) shows the orbitally resolved partial DOS for the L$\bar{3}$ TiO_2 layer. The electrons transferred from the AlO layer mainly occupy the Ti-3d_{xz} orbitals (about 77.1% of the electrons occupy these orbitals) and partially occupy Ti-3d_{xy} and Ti-3d_{yz} orbitals. This is different from LAO/STO heterostructures, where the preferential occupation of 2DEG is the in-plane Ti-3d_{xy} orbitals [47]. This anomalous behavior could be attributed to the contact of the interfacial Ti cations with the tetrahedral Al cations. The Al/TiO_2 interface breaks the perovskite lattice symmetry and changes the crystal field around the Ti ions near the interface. As a result, the energy of d_{xz}/d_{yz} orbitals is reduced and these orbitals become the preferable states for the electrons at the spinel-perovskite interface. The experimental results of Chikina *et al.* [48] and Cao *et al.* [49] also indicate that the energy of the d_{xz}/d_{yz} orbitals is less than that of the d_{xy} orbitals in GAO/STO heterostructures.

B. Influence of oxygen vacancies on the electronic structure of GAO/STO heterostructures

As mentioned in Sec. I, some researchers have suggested that the formation of 2DEG in GAO/STO heterostructures is caused by oxygen vacancies. Therefore, the effect of oxygen vacancies on the formation of 2DEG in GAO/STO heterostructures is further investigated. Considering that oxygen vacancies could be located in AlO, SrO, and TiO_2 layers, we construct $(\gamma\text{-}Al_2O_{2.96})_{2.25}/(SrTiO_3)_5$ heterostructures and $(\gamma\text{-}Al_2O_3)_{2.25}/(SrTiO_{2.95})_5$ heterostructures (each configuration contains only one oxygen vacancy in the supercell). First, we obtained the optimized structures of these configurations. All crystal structures experience similar structural distortions to that in configuration 1. Considering the GAO with Al layer termination at the interface, we calculate the formation energy (E_f) of oxygen vacancies using the relation

$$E_f = E_V - (E_0 - n_V \mu_O), \quad (1)$$

where E_V and E_0 are the total energies of the interface structure with and without oxygen vacancies, n_V is the numbers of oxygen vacancies, and μ_O is the chemical potential of oxygen atom. Figure 4 shows the formation energy as a function of the position of the oxygen vacancy. The square symbol represents the formation energy of the oxygen vacancy for the supercell containing only one oxygen vacancy. Inspection of Fig. 4 indicates that there are two energy minima; one lies in the L$\bar{3}$ TiO_2 layer and the other in the L6 AlO layer. The partial density of states projected onto atomic planes in the STO and GAO for an oxygen vacancy located in the L$\bar{3}$ TiO_2 layer (designated as configuration 2) and the L6 AlO layer (designated as configuration 3) is plotted in Figs. 5(a) and 5(b), respectively. For configuration 2, the top of the valence band also overlaps with the bottom of the conduction band, which is similar to that in configuration 1. Thus the 2DEG would also appear in the heterostructure with the structure of configuration 2. However, the 2DEG in configuration 2 is mainly located in the L$\bar{7}$ TiO_2 layer, which is different from that in configuration 1. In addition, the electrons transferred from the AlO layer mainly occupy the Ti-3d_{xy} orbitals. This is expected because the L$\bar{7}$ TiO_2 layer is far from the Al/TiO_2 interface and located deeply in the STO substrate. The carrier

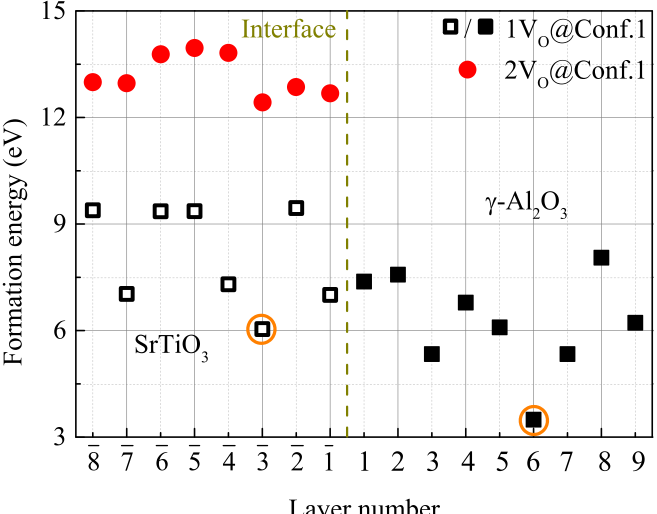

FIG. 4. Formation energies of oxygen vacancies at different atomic layers in configuration 1. The legend of $1V_O$@Conf. 1 represents one oxygen vacancy in the configuration 1; the other follows the same convention. For the configuration 1 containing two oxygen vacancies, one is fixed in the L6 AlO layer and the other varies at different atomic layers on the STO side. For the configuration 1 containing one oxygen vacancy, the circles mark the positions with the lower formation energy of the oxygen vacancy on the STO side and the GAO side.

concentration of configuration 2 is 5.18×10^{13} cm^{-2}, which is less than the concentration for fully compensating the polar electric field of GAO (1.47×10^{14} cm^{-2}). Two factors could be responsible for this phenomenon. (1) The oxygen vacancies in the L$\bar{3}$ layer could affect the lattice distortion near the interface and thus reduce the polar electric field. (The calculated polar field of configuration 2 is $\sim$0.24 V/Å, which is less than that of configuration 1. Correspondingly, the critical thickness of the GAO film for the existence of 2DEG should be $\sim$1.5 uc.) (2) The electrons released by the oxygen vacancies are found to form band gap states [marked by the solid arrow in Fig. 5(a)] and consequently have no contribution to the carrier concentration.

For configuration 3, there is no any overlap between the top of the valence band and the bottom of the conduction band [see Fig. 5(b)]. However, the Fermi level shifts upward into the conduction band, and the slab still reveals a metallic state in the band structure. Therefore, the 2DEG in configuration 3 does not originate from the polar discontinuity at the GAO/STO interface but from the oxygen vacancies in the GAO (similarly to modulation doping). An oxygen vacancy in the GAO/STO supercell could release one or two electrons to the STO [50,51]. This concentration of the transferred electron should vary from 1.57×10^{14} cm^{-2} to 3.14×10^{14} cm^{-2}. The carrier concentration of configuration 3 is 2.05×10^{14} cm^{-2} (Table I), indicating a partial ionization of the oxygen vacancies. The electrons transferred from the oxygen vacancy in the GAO are mainly accumulated in the L$\bar{3}$ TiO_2 layer. The value of the carrier concentration in configuration 3 is greater than that for fully compensating the polar electric field of GAO (1.47×10^4 cm^{-2}, as mentioned above). Thus, the polar electric field of GAO could be

TABLE I. Calculated carrier concentration n, average electron effective mass $\overline{m^*}/m_e$, $k\alpha$, and electron mobility μ of configuration 1, 2, 3, 5, and $(LAO)_5/(STO)_5$ heterostructures.

Configuration	n (cm^{-2})	$\overline{m^*}/m_e$	$k\alpha$	μ (cm^2/V s)
1	1.14×10^{14}	1.20	12.27	5.30×10^4
2	5.18×10^{13}	0.69	14.22	1.52×10^5
3	2.05×10^{14}	0.62	18.87	1.71×10^5
5	2.60×10^{14}	0.60	19.94	1.80×10^5
$(LAO)_5/(STO)_5$	1.32×10^{12}	2.81	3.630	1.74×10^4

completely compensated. This suggests that the formation of 2DEG in GAO/STO heterostructures would be irrelevant to the thickness of the GAO slab. Then, the electronic structures of $(\gamma\text{-}Al_2O_{2.87})_{0.75}/(SrTiO_3)_5$ and $(\gamma\text{-}Al_2O_{2.94})_{1.5}/(SrTiO_3)_5$ (containing only one oxygen vacancy in the supercell on the GAO side) are also calculated, and both of them exhibit metallic characteristics. Thus, there will be no critical thickness of GAO for the presence of 2DEG in the GAO/STO heterostructures when the oxygen vacancies are located on the GAO side. Experimentally, Chen *et al.* performed during-growth transport measurements for LAO/STO and related heterostructures and found that an amorphous film of less than 0.04 nm monolayer coverage on STO can already generate a highly conducting 2DEG [52]. The results demonstrate that the oxygen vacancies in GAO film grown on STO play an important role in generating 2DEG. We also calculate the electronic structures of the GAO/STO heterostructures with AlO and TiO_2 terminations and one oxygen vacancy in the supercell, and find that all configurations exhibit insulator characteristics in the band structure.

Now, we consider the situation that in the supercell both the GAO and the STO sides contain one oxygen vacancy, respectively. As the formation energy of the oxygen vacancy in the L6 AlO layer is the lowest (the filled square symbols in Fig. 4), we fix one oxygen vacancy in the L6 AlO layer and change the position of the other in the STO side for the $(\gamma\text{-}Al_2O_{2.96})_{2.25}/(SrTiO_{2.95})_5$ heterostructures. The formation energy variation with the position of the oxygen vacancy is also shown in Fig. 4 (the filled circle symbols), from which one can see that the formation energy does not change greatly with the change of oxygen vacancy position. This means that oxygen vacancies can be formed in any atomic layer on the STO side under low oxygen pressure.

Next, we focus on the electronic structures of $(\gamma\text{-}Al_2O_{2.96})_{2.25}/(SrTiO_{2.95})_5$ heterostructures. It is found that the $(\gamma\text{-}Al_2O_{2.96})_{2.25}/(SrTiO_{2.95})_5$ heterostructures show insulator characteristics in the band structure when the oxygen vacancy is located in the L$\bar{1}$, L$\bar{2}$, and L$\bar{3}$ layers, while for other cases, the heterostructures exhibit metallic characteristics. We take two configurations, in which the oxygen vacancy is in the L$\bar{3}$ TiO_2 layer (designated as configuration 4) and L$\bar{7}$ TiO_2 layer (designated as configuration 5), respectively, as examples to present the detailed results. The band structure of configuration 4 along high-symmetry lines in the Brillouin zone is plotted in Fig. 6(a). The Fermi level lies in the band gap, indicating that the 2DEG cannot be present in this configuration. Below the Fermi level, there are two discrete energy bands, which are designated as band 1 and band 2

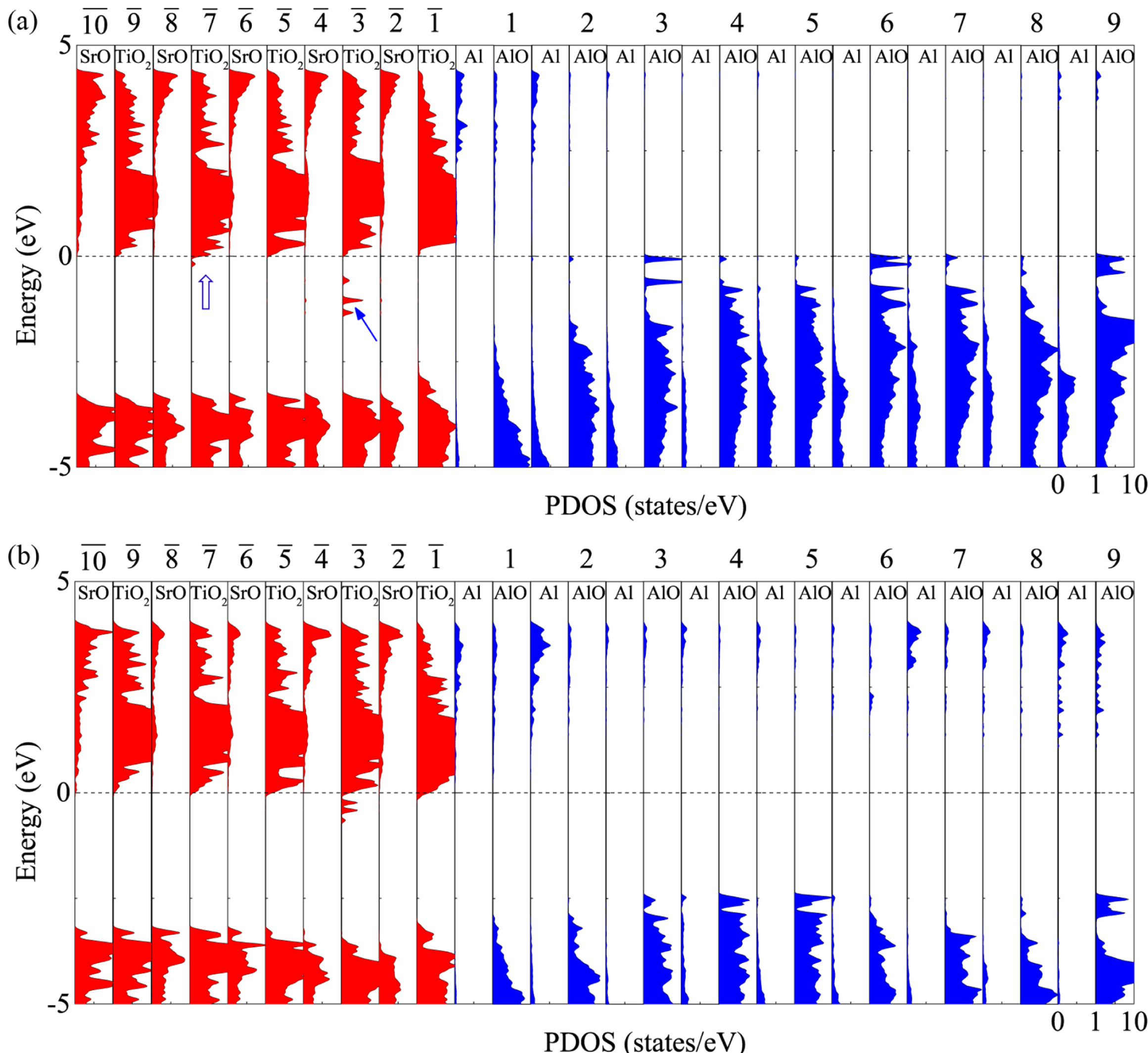

FIG. 5. The partial density of states projected onto atomic planes in the STO and GAO for (a) the $(\gamma\text{-}Al_2O_3)_{2.25}/(SrTiO_{2.95})_5$ heterostructures with one oxygen vacancy on the L$\bar{3}$ TiO_2 layer (configuration 2), and (b) the $(\gamma\text{-}Al_2O_{2.96})_{2.25}/(SrTiO_3)_5$ heterostructures with one oxygen vacancy on the L6 AlO layer (configuration 3). The hollow arrow in (a) marks the electron accumulation layer and the solid arrow points out the energy states of oxygen vacancies. The dash line represents the Fermi level.

[as indicated in Fig. 6(a)] for convenience. Figure 6(b) shows the **k**-resolved charge density isosurfaces for band 1 in the entire two-dimensional Brillouin zone. The charge density of band 1 exhibits a typical Ti-3d e_g-based bonding orbital characteristic, suggesting that the electrons are strongly localized at the oxygen vacancy and its adjacent Ti atoms [see L$\bar{3}$ layer in Fig. 6(b)]. It is indicated that band 1 corresponds to the impurity band introduced by oxygen vacancies, while band 2 is introduced by electrons transferred from GAO to STO, and the flat band shows that the electron effective mass is large. Figure 6(c) shows the **k**-resolved charge density isosurfaces for band 2. The charge density is located on one of the Ti atoms in the L$\bar{1}$ TiO_2 layer, showing a rather complex d-orbital composition. It could be composed of d_{xy}, d_{xz}, d_{yz}, $d_{3z^2-r^2}$, and $d_{x^2-y^2}$ orbitals. Thus, the electrons transferred from GAO to STO form localized states. In contrast to configuration 2 with only one oxygen vacancy in the L$\bar{3}$ layer, no 2DEG is formed in configuration 4 with an additional oxygen vacancy in the L6 layer. In fact, the additional oxygen vacancy could affect the crystal field near the Al/TiO_2 interface, which in turn causes the electrons transferred from GAO to STO to be localized.

Figure 6(d) illustrates the band structure of configuration 5. Unlike the electronic structure of configuration 4, the Fermi level for configuration 5 shifts upward into the conduction band, indicating that the 2DEG forms in heterostructures with this configuration. The bands introduced by the oxygen vacancies in STO and the electrons transferred from GAO to STO are also labeled as band 1 and band 2, respectively. Figures 6(e) and 6(f) show the **k**-resolved charge density isosurfaces for the two bands. From Fig. 6(e) one can see that the electrons in L$\bar{7}$ are localized at the oxygen vacancy and its adjacent Ti atoms, which is similar to that in L$\bar{3}$ layer of configuration 4. Thus the oxygen vacancies in the L$\bar{7}$ layer of STO are deep donors. Inspection of Fig. 6(f) indicates that the electrons transferred from GAO to STO are mainly located in the L$\bar{3}$ TiO_2 layer, occupy the Ti-3d_{xy} orbitals, and are uniformly distributed on each Ti atom. These electrons can

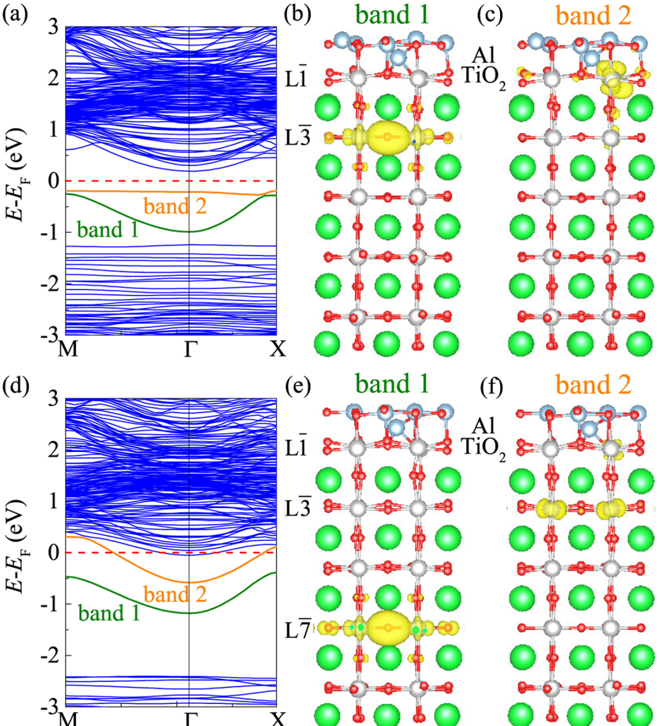

FIG. 6. (a) The band structure of $(\gamma\text{-Al}_2\text{O}_{2.96})_{2.25}/(\text{SrTiO}_{2.95})_5$ heterostructure with one oxygen vacancy in the L6 AlO layer and the other in the L$\bar{3}$ TiO_2 layer. (b) and (c) Partial charge density isosurfaces for band 1 and band 2. (d) The band structure of $(\gamma\text{-Al}_2\text{O}_{2.96})_{2.25}/(\text{SrTiO}_{2.95})_5$ heterostructure with one oxygen vacancy in the L6 AlO layer and the other in the L$\bar{7}$ TiO_2 layer. (e) and (f) Partial charge density isosurfaces for band 1 and band 2. The isosurface value is $0.045\,e/\text{Å}^3$.

move freely only in the L$\bar{3}$ TiO_2 layer, suggesting that the electrons transferred from GAO to STO are confined in the L$\bar{3}$ TiO_2 layer and form a 2DEG. It should be noted that only a few electrons transferred from GAO are localized around Ti atoms in certain positions in the L$\bar{1}$ layer, and the charge density isosurface region for each of these Ti atoms is far less than that of the corresponding Ti atom in configuration 4. Compared with the oxygen vacancies in the L$\bar{3}$ layer, the vacancies in the L$\bar{7}$ layer are farther away from the interface and have a weak effect on the crystal field near the Al/TiO_2 interface. Therefore, the electronic structure of configuration 5 is similar to that of configuration 3. The above results reveal that the formation of 2DEG in the GAO/STO heterostructures is closely related to the position of oxygen vacancies.

C. The electron mobilities in GAO/STO heterostructures

In the framework of the free-electron-like model, the mobility can be expressed as $\mu = e\langle\tau\rangle/m^*$, where e, τ, and m^* are the elementary charge, relaxation time, and electron effective mass, respectively. Besides the relaxation time, the effective mass plays an important role in determining the electron mobility. From the energy versus wave vector dispersion near the bottom of the conduction band, we obtain the electron effective masses along the Γ-M direction and the Γ-X direction. Then the average effective masses can be obtained using $\overline{m^*} = \sqrt{m^*_{\Gamma-\text{M}} m^*_{\Gamma-\text{X}}}$. The average effective masses for configurations 1, 2, 3, and 5 are listed in Table I. For comparison, we also calculated the band structure of the n-type LAO/STO heterostructure with configuration $(\text{LAO})_5/(\text{STO})_5$ (i.e., the five LAO layers are stacked on the five STO layers). Our results concerning the energy band of $(\text{LAO})_5/(\text{STO})_5$ are almost identical to those in Ref. [45]. The lowest band near the Γ point is composed of d_{xy} orbitals, and d_{yz} subbands show small dispersions from Γ to X points. The average effective mass of $(\text{LAO})_5/(\text{STO})_5$ is also given in Table I. For the GAO/STO heterostructures, the effective mass of configuration 1 is the largest, which is about 3/7 of that in $(\text{LAO})_5/(\text{STO})_5$, while there is little difference in effective masses of configurations 2, 3, and 5, which is about one-fourth of that in $(\text{LAO})_5/(\text{STO})_5$. Hence, the smaller effective masses must be one of the important reasons for the high mobility of 2DEG in GAO/STO heterostructures.

According to Christensen *et al.* [53], the electron mobility in GAO/STO heterostructures is governed by ionized impurity scattering in the low-temperature regime ($T < 5$ K). The ionized impurity scattering has been treated theoretically by Mansfield [54–57]. When the screen radius (α) is far greater than the wavelength of electrons (i.e., $k\alpha \gg 1$ with k being the wave vector), the ionized-impurities-scattering limited electron mobility can be expressed as [54–57]

$$\mu = \frac{3\epsilon^2 h^3 n}{16\pi^2 e^3 Z^2 N_i m^{*2} g(b)} \tag{2}$$

with

$$g(b) = \ln(1+b) - \frac{b}{1-b} \tag{3}$$

and

$$b = \frac{h^2\epsilon}{2e^2 m^*}\left(\frac{3n}{8\pi}\right)^{1/3}, \tag{4}$$

where ϵ is the dielectric constant, h is Planck's constant, n is the carrier concentration, Z is the charge of donors, and N_i is the concentration of charged donor centers. The screening radius α can be calculated by the Thomas-Fermi expression [56–58],

$$\alpha = \left[\frac{\hbar^2\epsilon}{4m^* e^2}\left(\frac{\pi}{3n}\right)^{1/3}\right]^{1/2}, \tag{5}$$

where $\hbar$ is the Planck's constant divided by 2π. The values of α were obtained by substituting the n, $\overline{m^*}$, and $\epsilon = 18\,000$ (STO) into Eq. (5). Taking $k = k_\text{F}$ with k_F being the Fermi wave vector, we obtain the values of $k\alpha$ and list them in Table I. Checking Table I indicates that the condition $k\alpha \gg 1$ is satisfied for each listed configuration. Since the charge donors are partially ionized, the values of Z and N_i are taken as 1 and n, respectively. Thus the electron mobility for each configuration is obtained and listed in Table I. The electron mobility in configuration 1 is about 3 times as large as that in $(\text{LAO})_5/(\text{STO})_5$, while the electron mobilities in heterostructures with configurations 2, 3, and 5 are ∼9, 10, and 11 times as large as that in $(\text{LAO})_5/(\text{STO})_5$. In addition, for the GAO/STO heterostructures, it is worth noting that there

is a certain distance between the electrons (forming 2DEG) and their donors in all configurations with 2DEGs. For example, in configuration 3, the 2DEG lies in the $L\bar{3}$ TiO_2 layer, which is 1.6 nm away from the oxygen vacancy lying in the L6 AlO layer. This is equivalent to realizing the modulation doping [25], which is a general way to suppress the donor scattering and improves the mobility in semiconductor technology. Therefore, the electron mobility in each GAO/STO heterostructure should be greater than the calculated value in Table I. The modulation doping, together with the smaller effective masses, explains why the higher mobility 2DEGs exist in the GAO/STO heterostructures (compared to LAO/STO heterostructures).

IV. CONCLUSIONS

In summary, the electronic structures of the [001]-oriented GAO/STO heterostructures with the TiO_2 layer terminated on the interfaces are systematically investigated by first-principles calculations. It is found that the necessary condition for the existence of 2DEG in the heterostructure is the device possessing an interface with TiO_2 and Al layer terminations. For GAO/STO heterojunctions without oxygen vacancies on the GAO side, the polar discontinuity near the interface is the main mechanism for the occurrence of 2DEG. When the oxygen vacancies are introduced into the GAO films, the polar electric field near the interface disappears and the oxygen vacancies become the main source of the 2DEG. In GAO/STO heterostructures the ionized impurity scattering is considered to govern the low-temperature mobility of the 2DEG, and it is found that the mobility in GAO/STO heterostructures with proper configurations can be one order of magnitude higher than that in LAO/STO heterostructures. The high mobility of the 2DEG is mainly due to the small electron effective mass in GAO/STO heterostructures.

ACKNOWLEDGMENTS

The calculation was conducted on the CJQS-HPC platform at Tianjin University. This work is supported by the National Natural Science Foundation of China through Grants No. 12174282 and No. 11774253.

[1] A. Ohtomo and H. Y. Hwang, A high-mobility electron gas at the $LaAlO_3/SrTiO_3$ heterointerface, Nature (London) **427**, 423 (2004).

[2] N. Nakagawa, H. Y. Hwang, and D. A. Muller, Why some interfaces cannot be sharp, Nat. Mater. **5**, 204 (2006).

[3] G. Herranz, M. Basletić, M. Bibes, C. Carrétéro, E. Tafra, E. Jacquet, K. Bouzehouane, C. Deranlot, A. Hamzić, J.-M. Broto, A. Barthélémy, and A. Fert, High Mobility in $LaAlO_3/SrTiO_3$ Heterostructures: Origin, Dimensionality, and Perspectives, Phys. Rev. Lett. **98**, 216803 (2007).

[4] A. Kalabukhov, R. Gunnarsson, J. Börjesson, E. Olsson, T. Claeson, and D. Winkler, Effect of oxygen vacancies in the $SrTiO_3$ substrate on the electrical properties of the $LaAlO_3/SrTiO_3$ interface, Phys. Rev. B **75**, 121404(R) (2007).

[5] C. Bell, S. Harashima, Y. Kozuka, M. Kim, B. G. Kim, Y. Hikita, and H. Y. Hwang, Dominant Mobility Modulation by the Electric Field Effect at the $LaAlO_3/SrTiO_3$ Interface, Phys. Rev. Lett. **103**, 226802 (2009).

[6] A. D. Caviglia, S. Gariglio, C. Cancellieri, B. Sacépé, A. Fête, N. Reyren, M. Gabay, A. F. Morpurgo, and J.-M. Triscone, Two-Dimensional Quantum Oscillations of the Conductance at $LaAlO_3/SrTiO_3$ Interfaces, Phys. Rev. Lett. **105**, 236802 (2010).

[7] A. D. Caviglia, M. Gabay, S. Gariglio, N. Reyren, C. Cancellieri, and J.-M. Triscone, Tunable Rashba Spin-Orbit Interaction at Oxide Interfaces, Phys. Rev. Lett. **104**, 126803 (2010).

[8] F. Gunkel, K. Skaja, A. Shkabko, R. Dittmann, S. Hoffmann-Eifert, and R. Waser, Stoichiometry dependence and thermal stability of conducting $NdGaO_3/SrTiO_3$ heterointerfaces, Appl. Phys. Lett. **102**, 071601 (2013).

[9] P. Perna, D. Maccariello, M. Radovic, U. Scotti di Uccio, I. Pallecchi, M. Codda, D. Marré, C. Cantoni, J. Gazquez, M. Varela, S. J. Pennycook, and F. M. Granozio, Conducting interfaces between band insulating oxides: The $LaGaO_3/SrTiO_3$ heterostructure, Appl. Phys. Lett. **97**, 152111 (2010).

[10] A. Annadi, A. Putra, Z. Q. Liu, X. Wang, K. Gopinadhan, Z. Huang, S. Dhar, T. Venkatesan, and Ariando, Electronic correlation and strain effects at the interfaces between polar and nonpolar complex oxides, Phys. Rev. B **86**, 085450 (2012).

[11] Y. Z. Chen, N. Bovet, F. Trier, D. V. Christensen, F. M. Qu, N. H. Andersen, T. Kasama, W. Zhang, R. Giraud, J. Dufouleur, T. S. Jespersen, J. R. Sun, A. Smith, J. Nygård, L. Lu, B. Büchner, B. G. Shen, S. Linderoth, and N. Pryds, A high-mobility two-dimensional electron gas at the spinel/perovskite interface of γ-$Al_2O_3/SrTiO_3$, Nat. Commun. **4**, 1371 (2013).

[12] D. V. Christensen, F. Trier, M. von Soosten, G. E. D. K. Prawiroatmodjo, T. S. Jespersen, Y. Z. Chen, and N. Pryds, Electric field control of the γ-$Al_2O_3/SrTiO_3$ interface conductivity at room temperature, Appl. Phys. Lett. **109**, 021602 (2016).

[13] S. W. Lee, J. Heo, and R. G. Gordon, Origin of the self-limited electron densities at $Al_2O_3/SrTiO_3$ heterostructures grown by atomic layer deposition—oxygen diffusion model, Nanoscale **5**, 8940 (2013).

[14] P. Schütz, F. Pfaff, P. Scheiderer, Y. Z. Chen, N. Pryds, M. Gorgoi, M. Sing, and R. Claessen, Band bending and alignment at the spinel/perovskite γ-$Al_2O_3/SrTiO_3$ heterointerface, Phys. Rev. B **91**, 165118 (2015).

[15] X. Yang, H. Su, and G. Wu, Orbital-adapted electronic structure and anisotropic transport in γ-$Al_2O_3/SrTiO_3$ heterostructure, Phys. Rev. Materials **4**, 016001 (2020).

[16] K. Wolff, R. Schäfer, M. Meffert, D. Gerthsen, R. Schneider, and D. Fuchs, Anisotropic electronic transport of the two-dimensional electron system in $Al_2O_3/SrTiO_3$ heterostructures, Phys. Rev. B **95**, 245132 (2017).

[17] N. Reyren, S. Gariglio, A. D. Caviglia, D. Jaccard, T. Schneider, and J.-M. Triscone, Anisotropy of the superconducting transport properties of the $LaAlO_3/SrTiO_3$ interface, Appl. Phys. Lett. **94**, 112506 (2009).

[18] N. Reyren, S. Thiel, A. D. Caviglia, L. F. Kourkoutis, G. Hammerl, C. Richter, C. W. Schneider, T. Kopp, A.-S. Rüetschi,

D. Jaccard, M. Gabay, D. A. Muller, J.-M. Triscone, and J. Mannhart, Superconducting interfaces between insulating oxides, Science **317**, 1196 (2007).

[19] A. D. Caviglia, S. Gariglio, N. Reyren, D. Jaccard, T. Schneider, M. Gabay, S. Thiel, G. Hammerl, J. Mannhart, and J.-M. Triscone, Electric field control of the $LaAlO_3/SrTiO_3$ interface ground state, Nature (London) **456**, 624 (2008).

[20] C. Cen, S. Thiel, G. Hammerl, C. W. Schneider, K. E. Andersen, C. S. Hellberg, J. Mannhart, and J. Levy, Nanoscale control of an interfacial metal-insulator transition at room temperature, Nat. Mater. **7**, 298 (2008).

[21] S. Thiel, G. Hammerl, A. Schmehl, C. W. Schneider, and J. Mannhart, Tunable quasi-two-dimensional electron gases in oxide heterostructures, Science **313**, 1942 (2006).

[22] J. A. Bert, B. Kalisky, C. Bell, M. Kim, Y. Hikita, H. Y. Hwang, and K. A. Moler, Direct imaging of the coexistence of ferromagnetism and superconductivity at the $LaAlO_3/SrTiO_3$ interface, Nat. Phys. **7**, 767 (2011).

[23] L. Li, C. Richter, J. Mannhart, and R. C. Ashoori, Coexistence of magnetic order and two-dimensional superconductivity at $LaAlO_3/SrTiO_3$ interfaces, Nat. Phys. **7**, 762 (2011).

[24] K. J. Kormondy, A. B. Posadas, T. Q. Ngo, S. Lu, N. Goble, J. Jordan-Sweet, X. P. A. Gao, D. J. Smith, M. R. McCartney, J. G. Ekerdt, and A. A. Demkov, Quasi-two-dimensional electron gas at the epitaxial alumina/$SrTiO_3$ interface: Control of oxygen vacancies, J. Appl. Phys. **117**, 095303 (2015).

[25] P. Schütz, D. V. Christensen, V. Borisov, F. Pfaff, P. Scheiderer, L. Dudy, M. Zapf, J. Gabel, Y. Z. Chen, N. Pryds, V. A. Rogalev, V. N. Strocov, C. Schlueter, T.-L. Lee, H. O. Jeschke, R. Valentí, M. Sing, and R. Claessen, Microscopic origin of the mobility enhancement at a spinel/perovskite oxide heterointerface revealed by photoemission spectroscopy, Phys. Rev. B **96**, 161409(R) (2017).

[26] T. Q. Ngo, N. J. Goble, A. Posadas, K. J. Kormondy, S. Lu, M. D. McDaniel, J. Jordan-Sweet, D. J. Smith, X. P. A. Gao, A. A. Demkov, and J. G. Ekerdt, Quasi-two-dimensional electron gas at the interface of γ-$Al_2O_3/SrTiO_3$ heterostructures grown by atomic layer deposition, J. Appl. Phys. **118**, 115303 (2015).

[27] S. W. Lee, Y. Liu, J. Heo, and R. G. Gordon, Creation and control of two-dimensional electron gas using Al-based amorphous oxides/$SrTiO_3$ heterostructures grown by atomic layer deposition, Nano Lett. **12**, 4775 (2012).

[28] Y. Z. Chen, N. Bovet, T. Kasama, W. W. Gao, S. Yazdi, C. Ma, N. Pryds, and S. Linderoth, Room temperature formation of high-mobility two-dimensional electron gases at crystalline complex oxide interfaces, Adv. Mater. **26**, 1462 (2014).

[29] G. Bridoux, M. Villafuerte, J. M. Ferreyra, N. Bachi, C. A. Figueroa, and S. P. Heluani, Light-induced metal-insulator transition in $SrTiO_3$ by photoresistance spectroscopy, Phys. Rev. B **92**, 155202 (2015).

[30] A. Samanta, W. E, and S. B. Zhang, Method for defect stability diagram from *ab initio* calculations: A case study of $SrTiO_3$, Phys. Rev. B **86**, 195107 (2012).

[31] K. van Benthem, C. Elsässer, and R. H. French, Bulk electronic structure of $SrTiO_3$: Experiment and theory, J. Appl. Phys. **90**, 6156 (2001).

[32] J. Lee and A. A. Demkov, Charge origin and localization at the *n*-type $SrTiO_3/LaAlO_3$ interface, Phys. Rev. B **78**, 193104 (2008).

[33] J. R. L. Mardegan, D. V. Christensen, Y. Z. Chen, S. Parchenko, S. R. V. Avula, N. Ortiz-Hernandez, M. Decker, C. Piamonteze, N. Pryds, and U. Staub, Magnetic and electronic properties at the γ-$Al_2O_3/SrTiO_3$ interface, Phys. Rev. B **99**, 134423 (2019).

[34] The electronic structures of STO slabs (the thickness $t = 5.5$, 9.5, and 12.5 uc) with identical top and bottom TiO_2 terminations, STO slabs ($t = 5.5$, 7.5, 9.5, and 15.5 uc) with identical top and bottom SrO terminations, and STO slabs ($t = 5$, 10, and 13 uc) with different terminations (one side terminated by SrO layer and the other side terminated by TiO_2 layer) are also calculated. The band gaps of TiO_2-terminated STO slabs and STO slabs with different terminations are almost identical ($E_g \simeq 2.25$ eV, being less than that of the bulk STO) and unchanged with increasing film thickness. In addition, the overall shape of the DOS spectra of the conduction band for each slab is similar to that of the bulk STO. However, spurious states would be introduced into the band gap of the STO slabs with identical top and bottom SrO terminations when $t \gtrsim 7.5$ uc. The $t = 5$ uc STO slab with different terminations is employed in our calculations.

[35] A. Vijay, G. Mills, and H. Metiu, Structure of the (001) surface of γ alumina, J. Chem. Phys. **117**, 4509 (2002).

[36] G. Gutiérrez, A. Taga, and B. Johansson, Theoretical structure determination of γ-Al_2O_3, Phys. Rev. B **65**, 012101 (2001).

[37] H. P. Pinto, R. M. Nieminen, and S. D. Elliott, *Ab initio* study of γ-Al_2O_3 surfaces, Phys. Rev. B **70**, 125402 (2004).

[38] C. Y. Ouyang, Ž. Šljivančanin, and A. Baldereschi, First-principles study of γ-Al_2O_3 (100) surface, Phys. Rev. B **79**, 235410 (2009).

[39] E. Menéndez-Proupin and G. Gutiérrez, Electronic properties of bulk γ-Al_2O_3, Phys. Rev. B **72**, 035116 (2005).

[40] S. Lu, K. J. Kormondy, T. Q. Ngo, T. Aoki, A. Posadas, J. G. Ekerdt, A. A. Demkov, M. R. McCartney, and D. J. Smith, Spectrum and phase mapping across the epitaxial γ-$Al_2O_3/SrTiO_3$ interface, Appl. Phys. Lett. **108**, 051606 (2016).

[41] D. Christensen and A. Smith, Is γ-Al_2O_3 polar?, Appl. Surf. Sci. **423**, 887 (2017).

[42] P. W. Tasker, The stability of ionic crystal surfaces, J. Phys. C: Solid State Phys. **12**, 4977 (1979).

[43] W. A. Harrison, E. A. Kraut, J. R. Waldrop, and R. W. Grant, Polar heterojunction interfaces, Phys. Rev. B **18**, 4402 (1978).

[44] M. Behtash, S. Nazir, Y. Wang, and K. Yang, Polarization effects on the interfacial conductivity in $LaAlO_3/SrTiO_3$ heterostructures: A first-principles study, Phys. Chem. Chem. Phys. **18**, 6831 (2016).

[45] W.-J. Son, E. Cho, B. Lee, J. Lee, and S. Han, Density and spatial distribution of charge carriers in the intrinsic *n*-type $LaAlO_3$-$SrTiO_3$ interface, Phys. Rev. B **79**, 245411 (2009).

[46] Y. Li, S. N. Phattalung, S. Limpijumnong, J. Kim, and J. Yu, Formation of oxygen vacancies and charge carriers induced in the *n*-type interface of a $LaAlO_3$ overlayer on $SrTiO_3$ (001), Phys. Rev. B **84**, 245307 (2011).

[47] A. Chikina, F. Lechermann, M.-A. Husanu, M. Caputo, C. Cancellieri, X. Wang, T. Schmitt, M. Radovic, and V. N. Strocov, Orbital ordering of the mobile and localized electrons at oxygen-deficient $LaAlO_3/SrTiO_3$ interfaces, ACS Nano **12**, 7927 (2018).

[48] A. Chikina, D. V. Christensen, V. Borisov, M.-A. Husanu, Y. Chen, X. Wang, T. Schmitt, M. Radovic, N. Nagaosa,

A. S. Mishchenko, R. Valentí, N. Pryds, and V. N. Strocov, Band-order anomaly at the γ-$Al_2O_3/SrTiO_3$ interface drives the electron-mobility boost, ACS Nano **15**, 4347 (2021).

[49] Y. Cao, X. Liu, P. Shafer, S. Middey, D. Meyers, M. Kareev, Z. Zhong, J.-W. Kim, P. J. Ryan, E. Arenholz, and J. Chakhalian, Anomalous orbital structure in a spinel-perovskite interface, npj Quantum Mater. **1**, 16009 (2016).

[50] C. Lin and A. A. Demkov, Electron Correlation in Oxygen Vacancy in $SrTiO_3$, Phys. Rev. Lett. **111**, 217601 (2013).

[51] A. Lopez-Bezanilla, P. Ganesh, and P. B. Littlewood, Magnetism and metal-insulator transition in oxygen-deficient $SrTiO_3$, Phys. Rev. B **92**, 115112 (2015).

[52] Z. Chen, M. Zhang, T. Ren, and Y. Xie, Unravelling oxygen-vacancy-induced electron transfer at $SrTiO_3$-based heterointerfaces by transport measurement during growth, J. Phys.: Condens. Matter **31**, 505002 (2019).

[53] D. V. Christensen, Y. Frenkel, P. Schütz, F. Trier, S. Wissberg, R. Claessen, B. Kalisky, A. Smith, Y. Chen, and N. Pryds, Electron Mobility in γ-$Al_2O_3/SrTiO_3$, Phys. Rev. Appl. **9**, 054004 (2018).

[54] O. N. Tufte and P. W. Chapman, Electron mobility in semiconducting strontium titanate, Phys. Rev. **155**, 796 (1967).

[55] D. Chattopadhyay and H. J. Queisser, Electron scattering by ionized impurities in semiconductors, Rev. Mod. Phys. **53**, 745 (1981).

[56] H. P. R. Frederikse and W. R. Hosler, Hall mobility in $SrTiO_3$, Phys. Rev. **161**, 822 (1967).

[57] A. Verma, A. P. Kajdos, T. A. Cain, S. Stemmer, and D. Jena, Intrinsic Mobility Limiting Mechanisms in Lanthanum-Doped Strontium Titanate, Phys. Rev. Lett. **112**, 216601 (2014).

[58] N. H. March, The Thomas-Fermi approximation in quantum mechanics, Adv. Phys. **6**, 1 (1957).